Extreme Mechanics Letters 15 (2017) 78–82

Contents lists available at ScienceDirect

Extreme Mechanics Letters

journal homepage: www.elsevier.com/locate/eml

Mechanics of electrochemically driven mechanical energy harvesting

Tianwu Chen [a], Hui Yang [a], Ju Li [b], Sulin Zhang [a,*]

[a] Department of Engineering Science and Mechanics, Pennsylvania State University, University Park, PA 16802, United States
[b] Department of Nuclear Science and Engineering and Department of Materials Science and Engineering, Massachusetts Institute of Technology, Cambridge, MA 02139, United States

ARTICLE INFO

Article history:
Received 8 May 2017
Accepted 5 June 2017
Available online 12 June 2017

Keywords:
Mechanical energy harvesting
Electrochemical cell
Stress–composition coupling
Finite-deformation kinematics
Chemical potential

ABSTRACT

Recent studies have demonstrated that an electrochemical cell can be mechanically activated and convert mechanical energy to chemical energy, thereby enabling a new class of electrochemically driven mechanical energy harvesters. Here we present a general mechanics framework to elucidate the stress–composition coupling and evaluate the performance of such mechanical energy harvesters. We obtained the functional dependence of the chemical potential of charge carriers on the chemical composition and mechanical deformation, which infers the capacity and open-circuit voltage. For a thin-film based electrochemical cell under bending, our analyses show that its capacity and open-circuit voltage depend on a set of design parameters, including applied curvature, initial composition, and the types of charge carriers (sodium versus lithium ions). We further developed a kinetic model with which we simulated the dynamic evolution of stress and composition in the thin-film cell. Our results provide fundamental guidance to optimize the performance of the mechanical energy harvesters.

1. Introduction

The abundant existence of mechanical energies in nature has attracted extensive interests in developing environmentally benign and sustainable mechanical energy harvesting technologies [1,2]. Despite the rapid advance in harvesting high-frequency (∼20–100 Hz) vibrational energies by exploiting piezoelectric [3], electrokinetic [4], or triboelectric effect [5,6], much less attentions have so far been drawn to harvest relatively low-frequency (∼0.5–5 Hz) mechanical energies [7,8], such as those embedded in everyday human activities. Our recent study has shown that asymmetric mechanical loading can drive charge-carrier migration between the two electrodes in an electrochemical cell, thereby converting mechanical energy to electric power [7]. The characteristic diffusion time scale of charge carriers endows relatively low operating frequencies (e.g. ∼1 Hz) of such power generators. Here we address the thermodynamics and kinetics of the stress-driven process in an electrochemical cell, which offers a fundamental guidance to the development and optimization of such electrochemically driven mechanical energy harvesters.

In an electrochemical cell, charge-carrier diffusion across the electrolyte can be both electrically and mechanically driven. In the latter case, asymmetric mechanical loading on the two electrodes, such as tension versus compression, gives rise to different chemical potentials of the charge carriers. The chemical potential difference drives dissociation of the charge carriers from one electrode, diffusion across the electrolyte, and insertion into the other electrode. Insertion/deinsertion of charge carriers induces chemical strain, accompanied by the mechanical deformation in the electrode materials. Within the finite-deformation kinematics, the total deformation gradient $\mathbf{F}$ is multiplicative of the chemical deformation gradient ($\mathbf{F}^c$) due to ion insertion and elastic deformation gradients ($\mathbf{F}^e$), as

$$\mathbf{F} = \mathbf{F}^e\mathbf{F}^c. \tag{1}$$

Here we assume that the electrodes operate in the elastic regime without causing plastic deformation. In the two-step deformation, a representative material point first deforms from the initial to an intermediate state by irreversible inelastic deformation and then further deforms elastically to the current state [9–11]. Accordingly, the elastic, chemical, and total strain tensors are

$$\mathbf{E}^e = \frac{1}{2}\left[\left(\mathbf{F}^e\right)^T\mathbf{F}^e - \mathbf{I}\right], \qquad \mathbf{E}^c = \frac{1}{2}\left[\left(\mathbf{F}^c\right)^T\mathbf{F}^c - \mathbf{I}\right],$$
$$E = \frac{1}{2}\left(\mathbf{F}^T\mathbf{F} - \mathbf{I}\right) = \left(\mathbf{F}^c\right)^T\mathbf{E}^e\mathbf{F}^c + \mathbf{E}^c. \tag{2}$$

For an electrode material B (such as silicon (Si) for a lithium (Li) cell or phosphorus (P) for a sodium (Na) cell), lithium/sodium insertion generates a phase A_xB (A = Li or Na; B = Si or P), such as Li_xSi or Na_xP. Let x_{max} be the maximum possible value of x, the concentration of A, defined as $c = x/x_{max}$, varies from 0 to 1. The chemical potential of A is $\mu = (\partial U/\partial N_A)_{\mathbf{F}}$, where U is the internal

* Corresponding author.
E-mail address: suz10@psu.edu (S. Zhang).

http://dx.doi.org/10.1016/j.eml.2017.06.002
2352-4316/

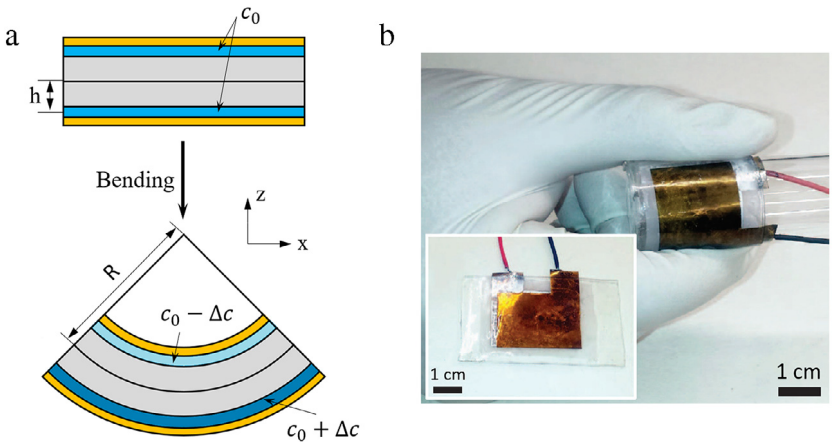

Fig. 1. The conceptual and actual mechanical energy harvester. (a) The cross-section of the device. The two electrodes (blue) with initial concentration c_0 are separated by the electrolyte (grey) with a distance h to the neutral plane. Current collectors (gold) are attached to the surfaces of the electrode materials. When a radius of curvature R is imposed, the ions in the compressed electrode are driven to the tensile side, resulting in the difference of concentration and the electric power. (b) The actual device in the bending and unbending (insert) conditions [7]. (For interpretation of the references to colour in this figure legend, the reader is referred to the web version of this article.)

energy and N_A is the mole number of the charge-carrier A under the fixed total deformation gradient $\mathbf{F}$. Let Π the internal energy density per unit volume, then $U = V_0 N_B \Pi$, where V_0 is the molar volume of A_xB at a reference concentration c_0, and N_B is the mole number of species B (the same as the mole number of A_xB). Note $x = N_A/N_B$, the chemical potential of A is

$$\mu = \frac{V_0}{x_{\max}} \left(\frac{\partial \Pi}{\partial c} \right)_{\mathbf{F}}. \tag{3}$$

Taking the total deformation gradient $\mathbf{F}$ and the concentration c as the independent variables, the internal energy density is comprised of the stress-independent and stress-dependent parts [10]

$$\Pi(\mathbf{F}, c) = \varphi(c) + J^c w(\mathbf{F}, c), \tag{4}$$

where the second term in Eq. (4) is the stress-dependent part. The elastic energy density $w(\mathbf{F}, c)$ is expressed in the intermediate state, and J^c is the Jacobian of the deformation gradient $\mathbf{F}^c$, i.e., the volume change when transforming an infinitesimal element from initial state to intermediate state. Since only the hydrostatic component of the elastic energy contributes to the chemical potential, $w(\mathbf{F}, c) = B\,\varepsilon_V^2/2$ [12], where B is the bulk modulus and $\varepsilon_V \equiv \mathrm{tr}(\mathbf{E}^e)$ is the trace of the elastic strain tensor, i.e., the elastic volumetric strain. The chemical potential can then be written as:

$$\begin{aligned} \mu(\mathbf{F}, c) &= \frac{V_0}{x_{\max}} \frac{\partial \varphi(c)}{\partial c} + \frac{1}{2} \frac{V_0}{x_{\max}} \\ &\quad \times \left(\frac{\partial J^c}{\partial c} B \varepsilon_V^2 + J^c \frac{\partial B}{\partial c} \varepsilon_V^2 + 2 J^c B \varepsilon_V \frac{\partial \varepsilon_V}{\partial c} \right)_{\mathbf{F}} \\ &= \mu_c + \mu_i + \mu_m + \mu_e, \end{aligned} \tag{5}$$

where μ_c, μ_i, μ_m, and μ_e are the chemical potential contributions from the changes in composition, volume, bulk modulus, and the elastic strain due to insertion of charge carriers, respectively. The first component μ_c induced by the compositional change of A is stress-independent, and can be also expressed as [10,13]

$$\mu_c(c) = \mu_0 + R_g T \log(\gamma c), \tag{6}$$

where μ_0 is a constant of the reference chemical potential and

$$\gamma = \frac{1}{1-c} \exp\left(\frac{1}{k_B T} \left[2(\alpha_0 - 2\beta_0) c - 3(\alpha_0 - \beta_0) c^2 \right] \right) \tag{7}$$

is the activity coefficient depending on concentration c and formation energy of A_xB. Here the activity constants, α_0 and β_0, relate to the formation energy, k_B is the Boltzmann constant, and T is the temperature. The other three terms in Eq. (5) are all stress-dependent. The chemical potential in Eq. (5) thus manifests the stress–composition coupling of the electrode.

The stress–composition coupling is active to all electrochemical devices [14–16]. Fig. 1 shows an example of such device in thin-film form, consisting of the two prelithiated Si (blue) electrodes with the initial concentration c_0. The Si electrodes are separated by the electrolyte (grey) and attached with current collectors (gold). Bending the thin film drives the charge carrier A to migrate and hence generates electric power if connected to an external circuit. Taking the initial state with concentration c_0 as the reference configuration, one has

$$\mathbf{F}^c = \left(J^c\right)^{\frac{1}{3}} \mathbf{I}, \qquad J^c = \frac{1 + \beta c}{1 + \beta c_0}, \tag{8}$$

where β is the volume changes from pure species B to $A_{x_{\max}}B$. Assuming Young's modulus of the mixed phase A_xB obeys the linear rule of mixture [17]: $Y(c) = Y_A V_A(c) + Y_B V_B(c)$, where Y_A and Y_B are Young's moduli of pure A and B, and V_A and V_B are volume fractions of species A and B, respectively. As the volume fraction depends on the concentration c, so as the Young's modulus of A_xB. Assuming the Poisson's ratio, ν, is weakly dependent on the concentration, one finds the bulk modulus $B(c) = Y(c)/[3(1-2\nu)]$.

When the energy harvester is subject to pure bending (Fig. 1), tensile and compressive strains, $\varepsilon_1 = \pm h/R$, are generated in the bottom and top electrodes, respectively, here h is the distance between the electrodes and the neutral plane of bending and R the radius of bending curvature (see Fig. 1). Under the plane-stress condition, the three principal strains are ε_1, 0, and $-\frac{\nu}{1-\nu}\varepsilon_1$. From Eqs. (2) and (8), the volumetric strain is $\varepsilon_V = \frac{1-2\nu}{1-\nu}(J^c)^{-2/3}\varepsilon_1 + \frac{3}{2}\left[(J^c)^{-2/3} - 1\right]$. Note that both $\varepsilon_1 \ll 1$ and $\left[(J^c)^{-2/3} - 1\right] \ll 1$. Let $\epsilon \equiv \max\left\{|\varepsilon_1|, \left|(J^c)^{-2/3} - 1\right|\right\}$, one finds $\varepsilon_V \sim O\|\epsilon\|$ and $\partial\varepsilon_V/\partial c \sim O\|\epsilon\|$. One follows that both μ_i and μ_m are $\sim O\left\|\epsilon^2\right\|$, and $\mu_e \sim O\|\epsilon\|$. Therefore, the chemical potential is mainly determined by $\mu \cong \mu_c + \mu_e$.

In the open-circuit condition, the asymmetric strain generated in the electrodes results in chemical potential difference (Fig. 1). Since the concentrations in the two electrodes are nearly unchanged in the open-circuit condition, the chemical potential difference is mainly contributed by the elastic effect. Specifically, $\Delta\mu \approx \Delta\mu_e = \left|\mu_e^- - \mu_e^+\right|$, where μ_e^- and μ_e^+ are the chemical potentials of the charge carriers in the compressive and tensile sides,

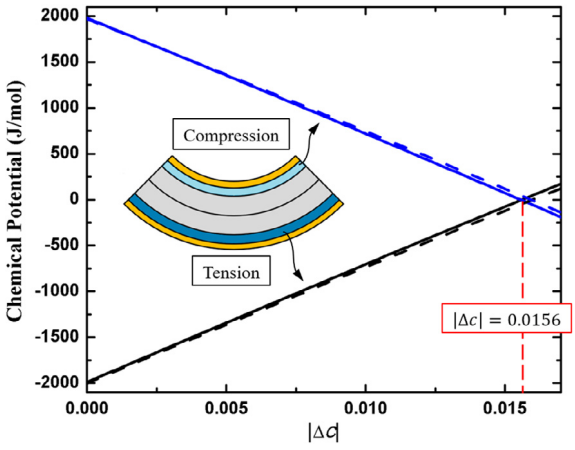

Fig. 2. The chemical potentials of the lithium ions in the compressed (blue solid line) and the stretched (black solid line) electrodes as a function of lithium concentration. The device is bent and hold at a radius of curvature $R = 0.63$ mm. The dash lines indicate the elastic chemical potential, μ_e, in the relative electrodes. (For interpretation of the references to colour in this figure legend, the reader is referred to the web version of this article.)

respectively. Since both μ_e^- and μ_e^+ linearly scale with ε_1, $\Delta\mu$ is inversely proportional to R. Therefore, the open circuit voltage can be expressed as $\Delta\phi = \Delta\mu_e/F \sim 1/R$ (F is the Faraday's constant). Taking Li_xSi as an example of composition A_xB, the Li_xSi electrodes are ~250 nm thick, covered by the polyimide layers and separated by the electrolyte. The device has the length of 3 cm and width of 2 cm. We set $h = 12.5$ μm and R to be the six different radii of curvature consistent with the experimental conditions [7], the voltages predicted by our model are listed in Table 2 and compared with those measured from the device prototype. Other relevant material properties and parameters are listed in Table 1.

In short-circuit condition, bending induced chemical potential difference between the two electrodes drives migration of lithium ions between the electrodes and thus charges the device. As shown in Fig. 2, when the device is bent to and held at a radius of curvature $R = 0.63$ mm, a large chemical potential difference is built between the two electrodes. As the lithium ions migrate from the compressed to the stretched electrode, the chemical potential difference induced by the elastic strain is counter-balanced by the concentration gradient and the system arrives at a new equilibrium at $\Delta c = 0.0156$.

The initial composition of the Li_xSi influences the performance of the energy harvester. Since $\Delta c \ll 1$, the chemical potential can be estimated as $\mu(\mathbf{F}; c) \cong \mu^0|_{\mathbf{F},c_0} + (d\mu/dc)_{\mathbf{F},c_0}\Delta c$. Since the chemical potential is dominated by μ_e, as shown in Fig. 2, then

$$\mu(\mathbf{F}; c) \cong \mu_e^0|_{\mathbf{F},c_0} + \left(\frac{d\mu_e}{dc}\right)_{\mathbf{F},c_0}\Delta c \cong \frac{V_B}{x_{\max}}B\beta\left[\frac{1-2\nu}{1-\nu}\varepsilon_1 - \frac{\beta}{1+\beta c_0}\text{sign}(\varepsilon_1)\,\Delta c\right]. \quad (9)$$

As shown in Fig. 3(a), given a radius of bending curvature R, the open-circuit voltage decreases nonlinearly as the initial concentration c_0 increases. Note that in an open circuit, $\Delta\mu \cong \Delta\mu_e = 2\mu_e^0|_{\mathbf{F},c_0}$. This follows that the nonlinearity arises from the nonlinear relation between the Young's modulus and the composition. In short-circuit situation, the two electrodes reach the chemical equilibrium, i.e., $\mu(\mathbf{F}, c_0 + \Delta c) = \mu(\mathbf{F}, c_0 - \Delta c)$ after ion migration that results in a compositional change of Δc. Then by Eq. (9),

$$\Delta c \cong \frac{1-2\nu}{1-\nu}\left(\frac{1}{\beta} + c_0\right)\varepsilon_1. \quad (10)$$

This suggests that the capacity of the device almost linearly depends on the initial concentration, c_0 (see Fig. 3(a)), despite the intrinsic nonlinear relationship between Δc (also the capacity) and c_0, as seen in Eq. (5). The linear relationship arises from the rather small concentration changes (Δc) in the electrodes at the chemical equilibrium.

The energy density stored in the harvester is the area between the blue and black solid lines in Fig. 2, which can be written as:

$$\Pi_{eff} = \int_0^{|\Delta c|}\Delta\phi\,\mathrm{d}Q = \frac{x_{\max}}{2V_0}\int_0^{|\Delta c|}\Delta\mu\,\mathrm{d}\,|\Delta c|\,. \quad (11)$$

The efficiency of the harvester is then $\eta = \Pi_{eff}/\Pi_{tot}$. Here $\Pi_{tot} = \boldsymbol{\sigma} : \mathbf{E}/2 = Y/[2(1-\nu^2)]\varepsilon_1^2$ is the bending energy density, where $\boldsymbol{\sigma}$ is the Cauchy stress tensor. Substituting Eqs. (9) and (10) in to Eq. (11), one finds the energy stored in the harvester, $\Pi_{eff} = \frac{1}{6}Y\varepsilon_1(1-2\nu)/(1-\nu)^2$, which gives the efficiency $\eta = \frac{1}{3}(1-2\nu)(1+\nu)/(1-\nu) = 27.8\%$. If also taking μ_i into account, the efficiency is slightly lower than 27.8% and gives the maximum efficiency, 27.15%, at $c_0 = 0.37$ (~$Li_{1.4}Si$), as shown in Fig. 3(b).

Black phosphorus (BP) is a promising high-capacity anode material for sodium ion batteries (NIBs), due to the significant cost advantage, the natural abundance of sodium precursors, and its stable pucker-layered structure [21]. Given the same loading strain, initial concentration, and volume of the electrodes, the open-circuit voltage and capacity of Na_xP as electrodes are compared, in Fig. 4, with those of Li_xSi. The material properties and parameters of Na_xP are also listed in Table 1. Because of its larger size, inserting a phosphorus atom into the electrode induces a larger volume change, and thus a higher value of $\partial\varepsilon_V/\partial c$. Since the chemical potential is dominated by the elastic part, μ_e, the open-circuit voltage is higher between the Na_xP electrodes (Fig. 4(a)) than the Li_xSi electrodes at the same applied radius of curvature. However, as shown in Fig. 4(b), with the same radius of the bending curvature, the Li_xSi energy generator has a higher capacity since the electrodes of the same volume and initial concentration can accommodate more lithium than sodium atoms due to the smaller molar volume of Li_xSi.

We next perform kinetics analysis of the thin-film energy harvester. The difference of the chemical potentials induces the ion flux between the electrodes across the electrolyte [22]:

$$\vec{J} = \vec{J_0} + \vec{J_s} = -D\vec{\nabla}c - \frac{Dc}{R_gT}\vec{\nabla}(\mu_i + \mu_m + \mu_e) \quad (12)$$

where D is the diffusion coefficient. R_g is the gas constant and T is the temperature. The first term on the right side of Eq. (12), in the form of classic Fick's law, is the stress-independent flux due to the concentration gradient, while the second term is the stress-dependent flux. Since the chemical potential due to the elastic effect (μ_e) is the dominant term in the stress-dependent chemical potential term, one has

$$\vec{J_s} \cong -\frac{Dc}{R_gT}\vec{\nabla}\mu_e = -\frac{D}{R_gT}\frac{V_B\beta c}{x_{\max}}\vec{\nabla}P \quad (13)$$

where $P = -B\,\varepsilon_V$ is the pressure, and $V_B = V_0/(1+\beta c_0)$. The ion migration is governed by the mass diffusion equation: $\partial c/\partial t = -\vec{\nabla}\cdot\vec{J}$.

Based on Eqs. (12) and (13), we set forth to simulate the bending/unbending cycling of the thin-film based electrochemical cell, integrating the mechanical and electrochemical processes. As shown in Fig. 5, two Li_xSi electrodes are separated by the electrolyte, with polyimide layers covered as protectors. The initial Li concentration is set as $c_0 = 0.827$ ($Li_{3.1}Si$, green in Fig. 5(a)). The thin film is first bent with a radius of curvature of $R = 0.63$ mm. Assuming the mechanical process is much faster than ion migration, bending/unbending and charging/discharging steps

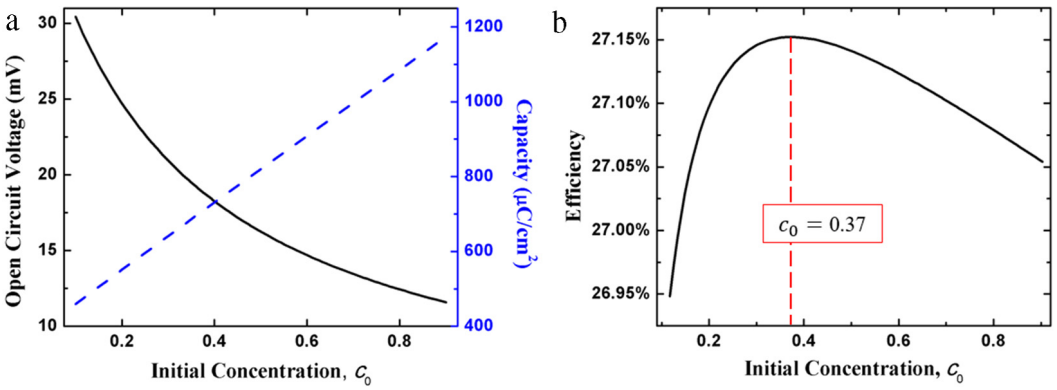

Fig. 3. (a) The open-circuit voltage (black solid line) and capacity (blue dash line), and (b) efficiency with different initial lithium concentrations in the electrodes. (For interpretation of the references to colour in this figure legend, the reader is referred to the web version of this article.)

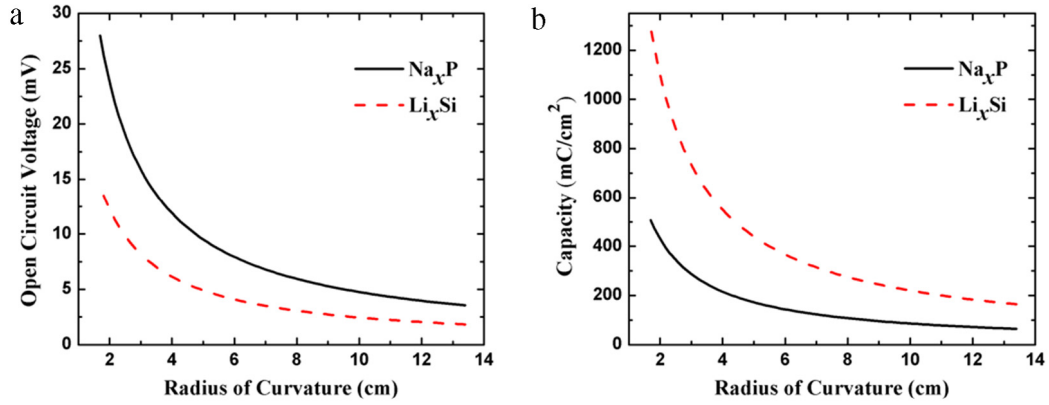

Fig. 4. The open circuit voltage (a) and capacity (b) of the Na_xP electrodes (black solid lines) and Li_xSi (red dash lines) at different radii of bending curvatures. (For interpretation of the references to colour in this figure legend, the reader is referred to the web version of this article.)

Table 1
Material properties and parameters of A_xB used in our model.

Properties and parameters of A_xB		Li_xSi	Na_xP
α_0	Activity constant	−0.31 eV/atom [18]	0.42 eV/atom [19]
β_0	Activity constant	−0.40 eV/atom [18]	−0.94 eV/atom [19]
Y_B	Elastic constant of pure species B	90 GPa [17]	70.3 GPa (BP) [20]
Y_A	Elastic constant of pure species A	5 GPa [17]	10 GPa
T	Temperature	300 K	
β	Volume change from pure B to $A_{x_{max}}B$	2.7	4.0
V_B	Molar volume of species B	1.21×10^{-5} m^3/mol	1.15×10^{-5} m^3/mol
x_{max}	Maximum concentration	3.75	3
ν	Poisson's ration	0.25	0.24
c_0	Initial concentration	0.827	

are uncoupled in our simulation. That is, mechanical equilibrium is always met during the charging/discharging process. As shown in Fig. 5(a), after the bending step, the central regions of electrodes are charged, with the Li concentrations increased to 0.843 in the stretched electrode and decreased to 0.811 in the compressed side ($\Delta c = 0.016$), which are comparable to the theoretical prediction in Fig. 2. Note that we assume that the electrodes are compositionally homogeneous in the theoretical analysis, while in the simulation Li concentration are nonuniformly distributed due to the pressure gradient inside each electrode. As shown in Fig. 5(b), after the unbending step, due to the expansion/shrinkage caused by the concentration changes, the charged side is in compression, while the discharged side is in tension. Therefore, the pressure difference drives ions back and consequently discharge the electrodes.

In conclusion, we present a theoretical model based on the stress–composition coupling to evaluate the electrochemically driven mechanical energy harvesters. Our energetics analysis shows that the chemical potential is dominated by the elastic effect, which follows that the open-circuit voltage is inversely proportional to the radius of bending curvature. The capacity in the charged electrodes almost linearly depends on the initial concentration, whereas the open-circuit voltage decreases nonlinearly

Table 2
The measured [7] and predicted voltages with different radii of bending curvatures.

Radius of curvature (mm)	$V_{measured}$ (mV)	$V_{predicted}$ (mV)
13.4	1.8	1.93
9.4	2.5	2.75
5.3	5.1	4.87
4.2	5.9	6.15
2.7	8.9	9.57
1.7	22.5	15.2

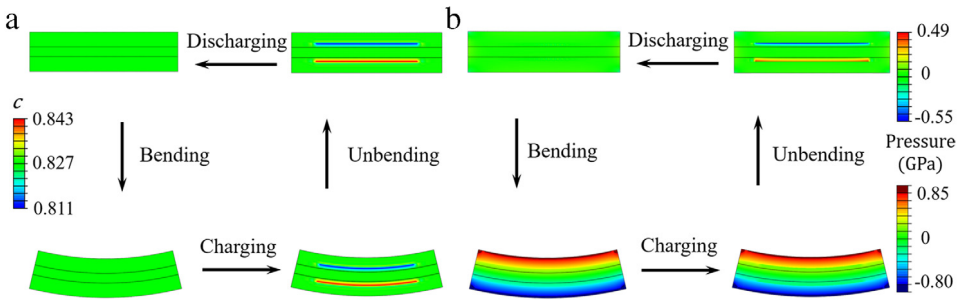

Fig. 5. The variances of (a) concentration and (b) pressure in the numerical model of electrodes which undergo the cycle of bending, charging, unbending and discharging with initial concentration $c_0 = 0.827$. (For interpretation of the references to colour in this figure legend, the reader is referred to the web version of this article.)

with the initial concentration. Compared to the Li_xSi electrodes, the Na_xP electrode based harvesters generate higher open-circuit voltage but lower capacity at the same initial concentration. We further simulate the bending/unbending cycling of a thin-film based electrochemical cell by the finite element method. The theoretical framework developed here is widely applicable to the stress–composition coupling effect under different loading conditions, and can easily extend to the plastic regime. Our findings provide rational guidance to the design of the new class of mechanical energy harvesters.

Acknowledgements

S. Z acknowledges the support by NSF ECCS-1610331, DMR-1610430 and CMMI-0900692. J. L. acknowledges the support by NSF ECCS-1610806.

References

[1] S. Xu, Y. Qin, C. Xu, Y.G. Wei, R.S. Yang, Z.L. Wang, Self-powered nanowire devices, Nature Nanotechnol. 5 (2010) 366–373.
[2] S.P. Beeby, M.J. Tudor, N.M. White, Energy harvesting vibration sources for microsystems applications, Meas. Sci. Technol. 17 (2006) R175–R195.
[3] S.R. Anton, H.A. Sodano, A review of power harvesting using piezoelectric materials (2003–2006), Smart Mater. Struct. 16 (2007) R1.
[4] M.-C. Lu, S. Satyanarayana, R. Karnik, A. Majumdar, C.-C. Wang, A mechanical-electrokinetic battery using a nano-porous membrane, J. Micromech. Microeng. 16 (2006) 667–675.
[5] F.R. Fan, Z.Q. Tian, Z.L. Wang, Flexible triboelectric generator!, Nano Energy 1 (2012) 328–334.
[6] D. Bhatia, W. Kim, S. Lee, S.W. Kim, D. Choi, Tandem triboelectric nanogenerators for optimally scavenging mechanical energy with broadband vibration frequencies, Nano Energy 33 (2017) 515–521.
[7] S. Kim, S.J. Choi, K. Zhao, H. Yang, G. Gobbi, S. Zhang, J. Li, Electrochemically driven mechanical energy harvesting, Nature Commun. 7 (2016) 10146.
[8] Y. Hou, Y. Zhou, L. Yang, Q. Li, Y. Zhang, L. Zhu, M.A. Hickner, Q. Zhang, Q. Wang, Flexible ionic diodes for low-frequency mechanical energy harvesting, Adv. Energy Mater. (2016) 1601983.
[9] A.F. Bower, P.R. Guduru, V.A. Sethuraman, A finite strain model of stress, diffusion, plastic flow, and electrochemical reactions in a lithium-ion half-cell, J. Mech. Phys. Solids 59 (2011) 804–828.
[10] Z.W. Cui, F. Gao, J.M. Qu, A finite deformation stress-dependent chemical potential and its applications to lithium ion batteries, J. Mech. Phys. Solids 60 (2012) 1280–1295.
[11] L. Chen, F. Fan, L. Hong, J. Chen, Y.Z. Ji, S.L. Zhang, T. Zhu, L.Q. Chen, A phase-field model coupled with large elasto-plastic deformation: Application to lithiated silicon electrodes, J. Electrochem. Soc. 161 (2014) F3164–F3172.
[12] M.T. McDowell, S.W. Lee, I. Ryu, H. Wu, W.D. Nix, J.W. Choi, Y. Cui, Novel size and surface oxide effects in silicon nanowires as lithium battery anodes, Nano Lett. 11 (2011) 4018–4025.
[13] H. Haftbaradaran, J. Song, W.A. Curtin, H.J. Gao, Continuum and atomistic models of strongly coupled diffusion, stress, and solute concentration, J. Power Sources 196 (2011) 361–370.
[14] B.W. Sheldon, S.K. Soni, X.C. Xiao, Y. Qi, Stress contributions to solution thermodynamics in Li-Si alloys, Electrochem. Solid State Lett. 15 (2012) A9–A11.
[15] M. Gu, H. Yang, D.E. Perea, J.G. Zhang, S.L. Zhang, C.M. Wang, Bending-induced symmetry breaking of lithiation in germanium nanowires, Nano Lett. 14 (2014) 4622–4627.
[16] H. Yang, W. Liang, X. Guo, C.-M. Wang, S. Zhang, Strong kinetics-stress coupling in lithiation of Si and Ge anodes, Extreme Mech. Lett. 2 (2015) 1–6.
[17] B. Hertzberg, J. Benson, G. Yushin, Ex-situ depth-sensing indentation measurements of electrochemically produced Si-Li alloy films, Electrochem. Commun. 13 (2011) 818–821.
[18] V. Shenoy, P. Johari, Y. Qi, Elastic softening of amorphous and crystalline Li–Si phases with increasing Li concentration: a first-principles study, J. Power Sources 195 (2010) 6825–6830.
[19] M. Mayo, K.J. Griffith, C.J. Pickard, A.J. Morris, Ab Initio study of phosphorus anodes for lithium- and sodium-Ion batteries, Chem. Mater. 28 (2016) 2011–2021.
[20] S. Appalakondaiah, G. Vaitheeswaran, S. Lebegue, N.E. Christensen, A. Svane, Effect of van der Waals interactions on the structural and elastic properties of black phosphorus, Phys. Rev. B 86 (2012) 035105.
[21] T. Chen, P. Zhao, X. Guo, S. Zhang, Two-fold anisotropy governs morphological evolution and stress generation in sodiated black phosphorous for sodium ion batteries, Nano Lett. 17 (2017) 2299–2306.
[22] R. Grantab, V.B. Shenoy, Pressure-gradient dependent diffusion and crack propagation in lithiated silicon nanowires, J. Electrochem. Soc. 159 (2012) A584–A591.